

# A study of plasma stability in the Imperial College Gabor lens and its application to focussing laser accelerated beams

Toby Nonnenmacher

June 20 2017

## Abstract

A Gabor lens is composed of a non-neutral plasma that is confined by an electric potential longitudinally and magnetic field radially. It may be used for the focusing of laser accelerated proton, ion, and electron beams . Its application may extend to usage in proton cancer therapy in the long term. In 2015, at a proton beam test at the University of Surrey, instabilities in the Imperial College Gabor lens plasma focussing the beam were observed. The work described here concerns studying the characteristics of the lens and ensuring it runs stably in future beam tests. It was found that a stable lens could be produced for base lens voltages ranging from 10 to 20kV below a critical magnetic field. Fourier space pictures showing the noise above the critical field are included here. Simulations of a proton beam travelling through the Imperial College Gabor lens were performed. Equivalent simulations for a muon beam were performed.

## Contents

<b>Abstract</b>	<b>1</b>
<b>1 Introduction to the Gabor lens</b>	<b>5</b>
<b>2 Gabor Lens Theory</b>	<b>6</b>
2.1 Focal length of the lens . . . . .	6

2.2	Paschen's Law . . . . .	7
<b>3</b>	<b>Motivations for the work</b>	<b>8</b>
<b>4</b>	<b>Parameters of the Imperial College Gabor lens</b>	<b>9</b>
<b>5</b>	<b>Gabor Lens Low Pressure Experimental Results</b>	<b>11</b>
5.1	Detector Results . . . . .	13
5.2	Stability of the Plasma . . . . .	15
5.3	Voltage Results . . . . .	15
<b>6</b>	<b>Gabor Lens Beam Simulation Results</b>	<b>17</b>
6.1	Simulation of a Proton Beam . . . . .	17
6.2	Simulation of a Muon Beam . . . . .	18
<b>7</b>	<b>Conclusions and Outlook</b>	<b>20</b>
	<b>References</b>	<b>21</b>

### Acknowledgements

In producing this work, I owe thanks to a number of people. I would like to thank Jürgen Pozimski, for his tireless supervision and advice throughout this work. I would also like to thank Piero Posocco for his help teaching me about the Gabor Lens, and Chung Lim Cheung for his assistance in the lab.

## List of Figures

1	Original schematic of the Gabor lens by D. Gabor. The electron cloud is constrained radially by the magnetic field produced by the coils, and longitudinally by the voltage of the anode. Gabor's lens required two magnetic fields in opposition and a hot cathode, unlike the Imperial College Gabor lens. figure taken from [1]. . . . .	5
2	Paschen's curve, showing breakdown voltage against the pressure multiplied by electrode gap length for 5 gases. At low pressures, $V_B$ rises sharply with decreasing pressure. At higher pressures, $V_B$ rises linearly with increasing pressure. . . . .	8
3	3D schematic of the Imperial College Gabor lens. The distance between the lens exit and the scintillator screen is 0.5m. If cooling is present, the operational range is 0–60kV, 0–45A. Figure taken from [12]. . . . .	10
4	Rings produced by 1 MeV proton pencil beam on the scintillator screen at 15kV for three different coil currents: 13.5A (left), 17A (centre), 22A (right). Figure taken from [12]. . . . .	10
5	Photograph of the voltage detector in the Gabor lens. The detector is composed of 16 segments, connected in groups of four, either in segments, left, or in concentric circles, right. . . . .	11
6	Schematic of the Gabor lens, current detector, and oscilloscope. The high voltage supply maintains the drop across the electrodes. Expelled ions hit the detector, and the current signal is converted to a voltage output signal in the oscilloscope. . . . .	12
7	Voltage signal read by the detector at different radial positions. Each channel represents one concentric circle of four detector segments, with Channel 1 corresponding to the innermost circle and Channel 4 the outermost. . . . .	13
8	Voltage signal read by the detector at different radial positions. Each channel represents one quarter segment of the circle combining 4 detector segments, with Channel 2 and 3 composing the right half of the detector, and Channel 1 and 4 the left half. . . . .	14
9	Simulations of the output of the detector at different radial positions. The cone of ions falling on the detector is simulated as being gaussian, with radius 10mm, left, 30mm, centre, and 90mm, right. . . . .	14
10	Fourier transform of the voltage signal for no plasma, left, and plasma in the voltage limited regime, right. The magnitude of noise is the same in both plots. . . . .	15

11	Fourier transform of the voltage signal for the plasma in the current limited regime above the critical magnetic field strength. The full frequency range is shown, left, and the low frequency range, right. A large increase in noise is visible in the low frequency range. . . . .	16
12	Sensor voltage against current through the coils for a base voltage of 14kV. The lowest input current is slightly below the limit for plasma to be produced, and the plot ends at the critical magnetic field. Above this, the plasma became unstable, and no further voltage readings could be taken. The results from all four channels of the voltage sensor are shown. . . . .	16
13	Sensor voltage against current through the coils for a range of base voltages 10 to 20kV. . . . .	17
14	Results of the simulation of a proton beam travelling through the Gabor lens, a beam pipe, and aperture. The Gabor lens ranges from 0 to 0.59m in the z direction and the aperture is placed at 1.09m. The protons range in energy from 0.1MeV, in blue, to 7.4MeV in red. . . . .	18
15	Energy histogram of particles at $z = 1.2\text{m}$ , just beyond the aperture. The energies of the particles are given in terms of their Lorentz factor. Two sets of particles have survived, with average energies 0.47MeV and 2.25MeV respectively. . . . .	19
16	Density of muons travelling through the Gabor lens and beam pipe. The Gabor lens ranges from 0 to 0.59m in the z direction. The highest density, in red, occurs at the focal spot, at 2.0m from the end of the lens. . . . .	19

## 1 Introduction to the Gabor lens

The Gabor lens, or space-charge lens, is an axially symmetric beam optics device, based on a non-neutral plasma, confined by both a high electric potential longitudinally, and a uniform magnetic field radially. In the setup, originally proposed by Gabor in 1947, the longitudinal magnetic field is produced by two coils, and radially restricts the electrons composing the plasma [1]. The voltage drop is provided by a circular cathode near the magnetic field line that crosses the axis, and a cylindrical anode in the area of axial magnetic field. This drop constrains the electrons longitudinally, such that the electrons are contained from all directions. If the magnetic field is too high, electrons in the lens experience too strong an inward force and discharges between the anode and ground may occur. In this instance, the plasma changes from a regime in which it is limited by the voltage to one in which it is limited by the current.

The non-neutral plasma is initially produced within the lens, by filling the lens with electrons, which can occur by one of three mechanisms [2]: Collisional ionisation of beam ions by residual gas, production from a gas discharge, or by a hot cathode (as in the original Gabor lens). The plasma produced causes strong cylindrically-symmetric focusing of the oppositely charged beam, beyond the capability of any conventional lens system. A schematic of the Gabor lens is given in figure 1. For a base voltage of 20kV, the Gabor lens has a focal length on the order of metres

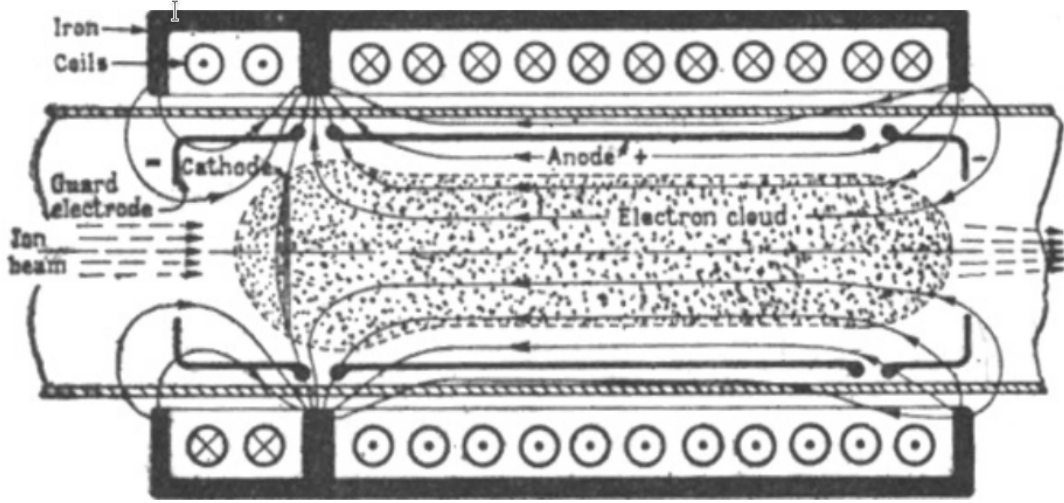


Figure 1: Original schematic of the Gabor lens by D. Gabor. The electron cloud is constrained radially by the magnetic field produced by the coils, and longitudinally by the voltage of the anode. Gabor's lens required two magnetic fields in opposition and a hot cathode, unlike the Imperial College Gabor lens. figure taken from [1].

for a 1MeV proton beam.

## 2 Gabor Lens Theory

### 2.1 Focal length of the lens

The electrons in the plasma within the lens are distributed evenly with a space-charge density given by equation 1, where  $e$  and  $m_e$  are the charge and rest mass of the electron respectively,  $B_z$  is the z component of the magnetic field, and  $\epsilon_0$  is the permittivity of free space:

$$\rho_{e,max} = \frac{e\epsilon_0 B_z^2}{2m_e}. \quad (1)$$

The electrons rotate around the axis in the steady state.

The focusing force on a positive ion beam is produced by the space charge of the electron cloud inside the chamber. The focal length of the lens is derived from the equation of motion for the electrons inside the plasma, Gauss' law, and the momentum equation given in equation 2:

$$n_e m_e \frac{d\bar{v}_e}{dx} = -n_e e (\bar{E} + \bar{v}_e \times \bar{B}) - \nabla P_e; \quad (2)$$

where  $-n_e e (\bar{E} + \bar{v}_e \times \bar{B})$  is the Lorentz force acting on the electron from the electromagnetic field inside the lens, and  $\nabla P_e$  is the pressure[3]. The maximum longitudinal electron density,  $n_l$ , that can be confined by the electrostatic field is given in equation 3 [4]:

$$n_l = \frac{4\epsilon_0 V_c}{er_c^2}; \quad (3)$$

where  $r_c$  and  $V_c$  are the radius and potential of the cylindrical electrode, respectively. The maximum radial electron density,  $n_r$ , that can be confined by the axial magnetic field  $\bar{B} = B_0 \hat{z}$  is given in equation 4 [4]:

$$n_r = \frac{\epsilon_0}{2m_e} B^2. \quad (4)$$

By equating the radial and longitudinal electron densities, the threshold potential for electrons flowing to the anode in the presence of the magnetic field, given in equation 5, can be calculated as:

$$V_c = \frac{er_c^2}{8m_e} B^2. \quad (5)$$

Combining equation 4 and the equation for the force on a charged particle, the focusing force may be given, as in equation 6 [4]:

$$\bar{F}_f = -\frac{em_i}{8m_e} \frac{B^2}{U_B} \hat{r}; \quad (6)$$

where  $U_B$  is the accelerating potential of the ions, equal to the energy over charge,  $\frac{m_i v^2}{2q}$ , and  $m_i$  and  $v$  the mass and longitudinal velocity of the ion respectively [5]. The focal length,  $f$ , of the Gabor lens is then given by equation 7 [4]:

$$\frac{1}{f} = -\frac{e}{8m_e} \frac{B^2}{U_B} L; \quad (7)$$

where  $L$  is the length of the lens.

The focal length of the Gabor lens is, therefore, proportional to the energy of the ion, in contrast to the focal length of an electrostatic quadrupole which is proportional to the square root of the energy of the ion [4].

This holds under equilibrium conditions in which the rate of electron production and expulsion are equal, with the majority of the electrons confined within the lens. Under these conditions, electrons cannot reach the anode and the high voltage supply acts as a potential divider providing voltage to the anode split between the internal resistance of the high voltage power supply, and the resistance of the plasma. In this voltage controlled regime the anode receives the entirety of the voltage provided by the high voltage supply as the internal resistance is negligible, and there is a stable potential difference between the anode and ground electrode. However, if the magnetic field is increased above a critical value, the plasma resistance falls. The current regime is entered, the electrons escape to the anode. Given the focal length, the average electron density when a beam of energy  $E_{beam}$  passes through the lens is given in equation 8:

$$n_e = \frac{4\epsilon_0 E_{beam}}{ef} L. \quad (8)$$

For a steady state plasma, the rate of electron production is equal to the rate of electron expulsion with the majority of the electrons confined within the chamber [6].

The current emitted from the plasm in the lens is given by 9::

$$I = \sigma v_e V_{tank} n_{RGA} \frac{n_e}{e}; \quad (9)$$

where  $\sigma$  is the interaction cross-section between the electrons and gas,  $v_e$  is the velocity of the electrons,  $V_{tank}$  is the total volume of the tank, and  $n_{RGA}$  and  $n_e$  are the densities of residual gas atoms and electrons respectively. It is therefore possible to calculate the electron density within the lens from measurements of the current emitted.

## 2.2 Paschen's Law

Paschen's law relates the the voltage necessary to cause a discharge between two electrodes in a gas to the gap length and the pressure. A graph of the Paschen curve, given in figure 2. Below a critical pressure, the breakdown voltage required for a discharge increases with decreasing pressure. Above this minimum, the increase in breakdown voltage is close to linear with pressure. The equation for the breakdown voltage,  $V$ , is given in equation 10: [7]

$$V = \frac{apd}{\ln pd + b}; \quad (10)$$

where  $p$  is the pressure,  $d$  the gap distance between the electrodes, and the constants  $a$  and  $b$  depend on the composition of the gas, which determines both the minimum arc voltage and the

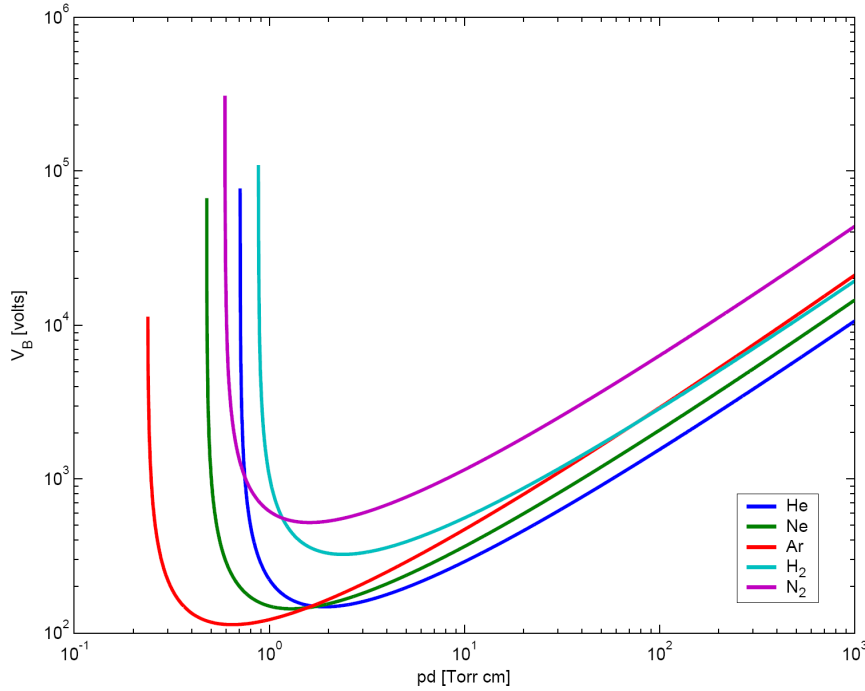


Figure 2: Paschen's curve, showing breakdown voltage against the pressure multiplied by electrode gap length for 5 gases. At low pressures,  $V_B$  rises sharply with decreasing pressure. At higher pressures,  $V_B$  rises linearly with increasing pressure.

distance at which it occurs. In the absence of collisional ionisation and a magnetic field, the mean free path between the electrodes is equal to the shortest distance between them. However due to the collisions with residual gas molecules, and the presence of a magnetic field, the actual distance the electrons travel between the electrodes is significantly longer.

### 3 Motivations for the work

Laser based accelerators producing ion, proton, and electron beams are increasingly finding uses as an alternative to conventional accelerators, such as synchrotrons and cyclotrons. Major advantages of laser based accelerators are their relative size and cost, being much smaller and cheaper than a synchrotron or cyclotron at equivalent energies. The reduction in size stems from the wavelength of the EM wave being approximately  $10^6$  times shorter than that of a conventional accelerator [8]. The Gabor lens is the ideal partner of laser-accelerated beams due its ability to reach high focusing with a low magnetic field compared with conventional solutions. For example, for a 25MeV proton beam, in order to achieve a focal length of 1m the required field is 0.06T for a Gabor lens of 0.3m, in contrast with 2.6T for a solenoid with the same effective length. This is particularly important when beams are produced with a large divergence angle [9].

While laser based systems cannot yet access energies available using conventional accelerators,



laser technology is improving. In the last 10 years, laser driven accelerators have been shown to be capable of producing beams of energy 60MeV, with a predicted increase of at least a factor of 5 to 10 [4].

One possible future application of a beam accelerated by a laser and focused by a Gabor lens is in proton beam therapy. Proton beam therapy is an alternative to conventional radiation therapy, first proposed in 1946 by Robert R. Wilson. The main advantage of proton therapy is its superior spatial dose distribution in the patient [10]. The energy distribution of a proton provides a uniform and highly conformal dose to a tumour. This reduces the damage caused to surrounding normal tissues in comparison with conventional radiotherapy, in which photons lose much of their energy before reaching the tumour [11].

The decrease in damage to healthy tissue makes proton therapy particularly important in the treatment of cancers of the eye, skull base, and spine, along with paediatric cancers. 56 proton therapy centres currently exist worldwide, spanning North America, Europe, and Asia.

To treat deep seated tumours, proton beams with a maximum energy around 250MeV or beams of carbon ions with up to 450MeV per nucleon are required. If a laser driven proton accelerator focused by a Gabor lens could produce beams of these energies, it could provide a substantial reduction in size and cost when compared with a synchrotron. The compact size of a lattice of such a lens would allow the attachment of the full acceleration and delivery system to be mounted on the gantry, for faster treatment at reduced cost. Applications in the shorter term, on the road to proton beam therapy, include Radiobiological Experiments at lower energies. These encompass both in vitro proton beams on single cell layers and in vivo proton beams on  $\sim 1\text{cm}^3$  tumors in mice at energies of 3MeV and 30MeV respectively. In addition to proton and ion beams, a Gabor lens may find application in focussing muon beams. A preliminary study into simulating muon beams focussed by the Gabor lens are discussed in Section 6.2.

## 4 Parameters of the Imperial College Gabor lens

A Gabor lens prototype operating at high electron density was built at Imperial College London and tested at the Ion Beam Centre of the University of Surrey with a 1 MeV proton beam in 2015. A schematic of the lens is provided in figure 3. The lens has a total length of 540mm, much smaller than a conventional accelerator, and uses a high electron density of about  $5 \times 10^{-7}\text{C m}^{-3}$ . The central electrode has an inner diameter of 66mm and an outer diameter of 89mm. The maximum magnetic field achieved at 45A is approximately 55mT. During testing at the University of Surrey, rather than simply over- or underfocusing, the lens unexpectedly converted incoming pencil beams into rings. The rings are shown in figure 4, and the radius of the rings depended on the lens settings. Additionally, periodic features appeared along the circumference, suggesting that the electron plasma was excited into an unstable state. Much of the subsequent work has been concerned with discovering the cause of the formation of rings. One possible cause which

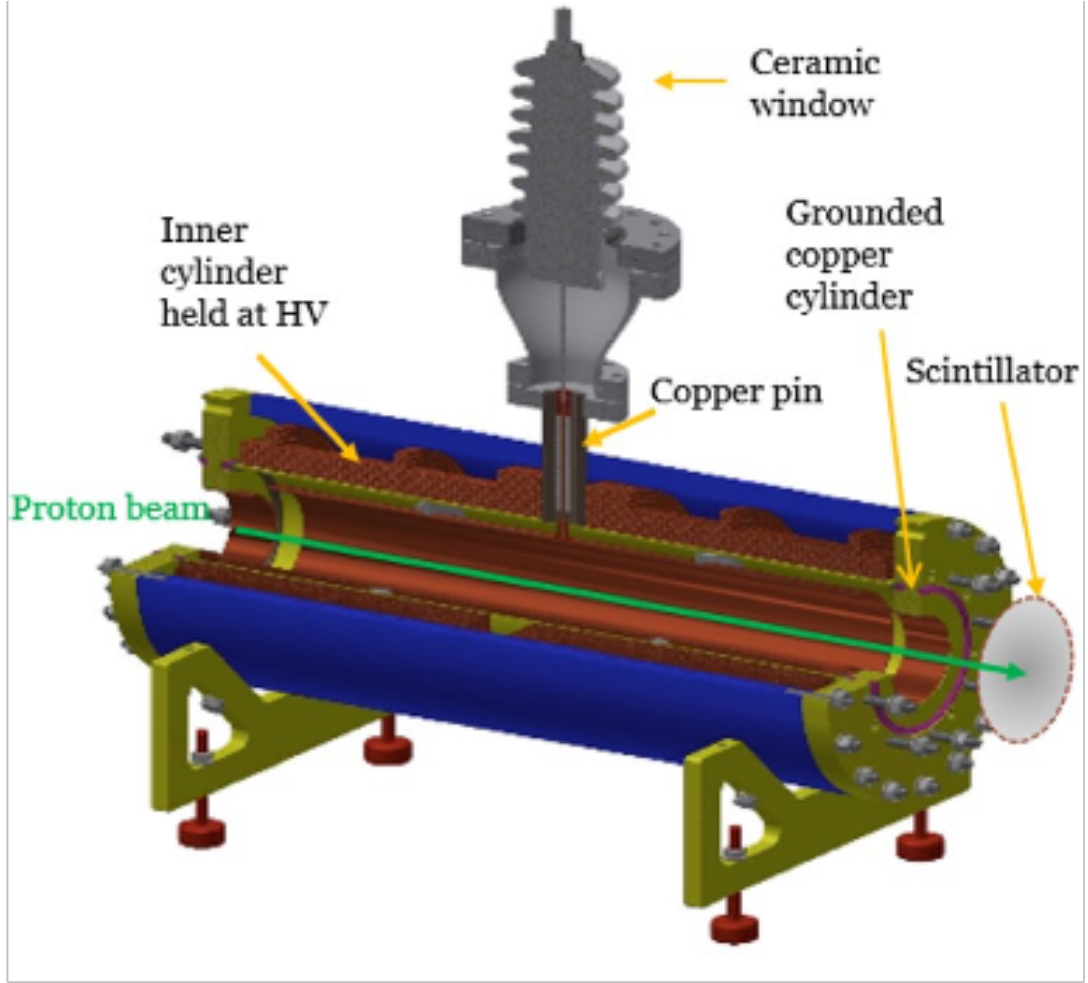


Figure 3: 3D schematic of the Imperial College Gabor lens. The distance between the lens exit and the scintillator screen is 0.5m. If cooling is present, the operational range is 0–60kV, 0–45A. Figure taken from [12].

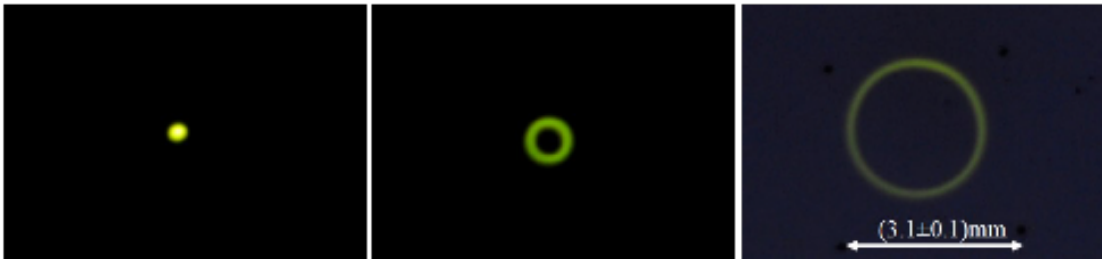


Figure 4: Rings produced by 1 MeV proton pencil beam on the scintillator screen at 15kV for three different coil currents: 13.5A (left), 17A (centre), 22A (right). Figure taken from [12].



Figure 5: Photograph of the voltage detector in the Gabor lens. The detector is composed of 16 segments, connected in groups of four, either in segments, left, or in concentric circles, right.

was seen by Neuner in 2000 is a high-current electron discharge on the axis of the lens causing over- or underfocusing of the beam [13]. This can be ruled out in this case, as no discharge was present when the rings were produced. Further improvements have already been made to correct the magnetic field, by correcting the winding coils. These caused too great a drop in magnetic field away from the centre of the lens, and therefore needed to be ruled out as a cause of the instability observed.

One possibility to be investigated was that the rings may have been caused by instability in the plasma due to running at too high a pressure. Therefore the Imperial College lens setup was improved to reduce the pressure from  $1.6 \times 10^{-6}$  mbar to  $3.0 \times 10^{-7}$  mbar. This reduction in pressure increases the voltage required for a discharge between the electrodes to occur in accordance with the Paschen curve discussed in Section 2.2. The data taken at this reduced pressure are presented in Section 5.

## 5 Gabor Lens Low Pressure Experimental Results

Data was taken using a voltage sensor, which detects the current of discharging ions and electrons and multiplies it by the input resistance to give a voltage reading. The detector was composed of 16 adjustable segments, 0.57m from the end of the lens, read into a 4-channel oscilloscope. The detector segments were connected in either concentric circle or sector arrangement as shown in figure 5. The base voltage and the current through the magnetic coils were varied, along with the position of the voltage sensor. The pressure in the tank could also be varied, but was kept at a minimum for all of the following results. It was discovered that temperature had a significant effect on the performance of the lens, so a water cooling system was introduced to minimise the increase of temperature during lens operation.

A simple schematic of the lens and detector system is given in figure 6. The voltage results for

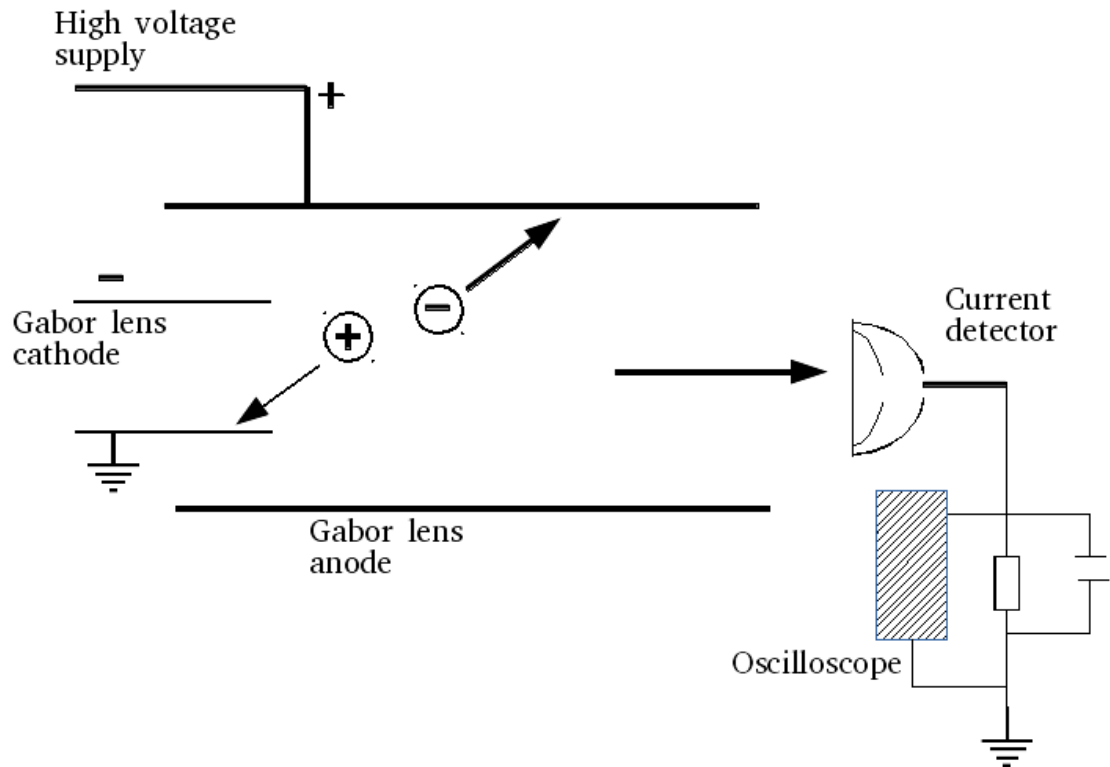


Figure 6: Schematic of the Gabor lens, current detector, and oscilloscope. The high voltage supply maintains the drop across the electrodes. Expelled ions hit the detector, and the current signal is converted to a voltage output signal in the oscilloscope.

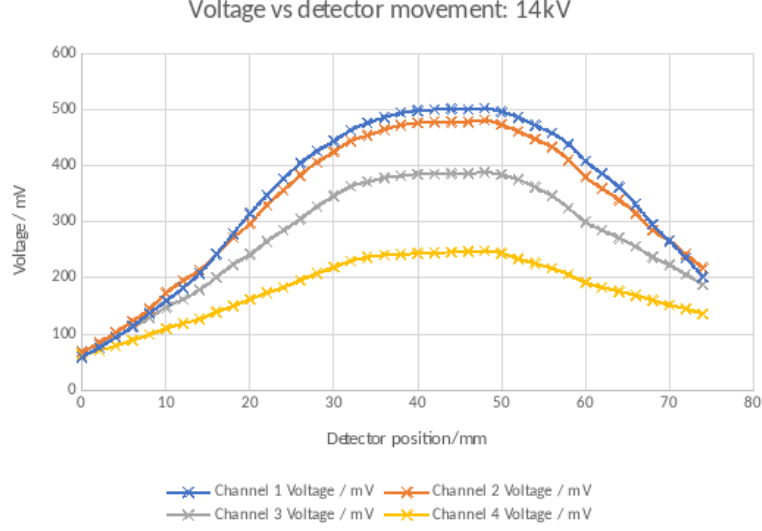


Figure 7: Voltage signal read by the detector at different radial positions. Each channel represents one concentric circle of four detector segments, with Channel 1 corresponding to the innermost circle and Channel 4 the outermost.

variation of base voltage, magnetic field, and sensor position, as well as noise results in different plasma regimes are given and discussed in this section.

### 5.1 Detector Results

As the residual gas atoms are ionised, the positive ions accelerate in both the longitudinal and radial directions. Ions are accelerated radially towards the zero potential at the axis due to the voltage drop. As the collisional ionisation occurs homogeneously, in the radial direction, the radial velocity is a rectangle function with respect to radius [14]. The ions are accelerated longitudinally towards the ground electrode. The ions are more easily stripped of electrons in between the electrodes, so ionisation is more likely in this region. Therefore, the longitudinal velocity is a Gaussian function with respect to the longitudinal distance on the axis. The convolution of these forms a bell-shaped distribution and the ions leave the plasma distributed across a cone.

This was demonstrated by varying the position of the voltage detector. The detector was moved across a range of 75mm transverse to the axis of the lens. With a plasma present, confined by the electric and magnetic fields in the stable voltage limited regime, the detector was extended across the full range, with voltage data taken every 2mm. These measurements, taken with the detector wired first in the radial arrangement, then in the sector arrangement, are presented in figures 7 and 8.

In the concentric circle arrangement, the bell shaped pattern, characteristic of the cone of

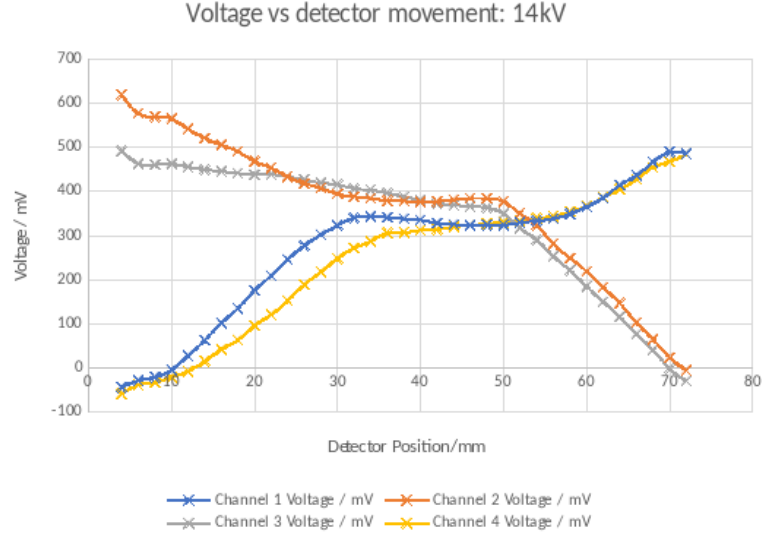


Figure 8: Voltage signal read by the detector at different radial positions. Each channel represents one quarter segment of the circle combining 4 detector segments, with Channel 2 and 3 composing the right half of the detector, and Channel 1 and 4 the left half.

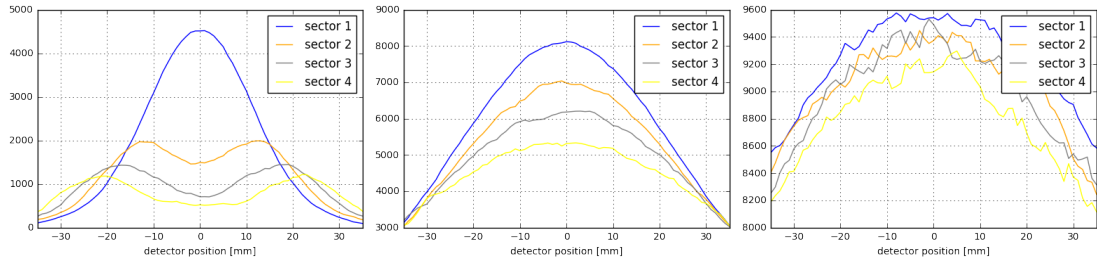


Figure 9: Simulations of the output of the detector at different radial positions. The cone of ions falling on the detector is simulated as being gaussian, with radius 10mm, left, 30mm, centre, and 90mm, right.

ions, is observed. The distribution implies that the radius of the cone hitting the detector is smaller than the radius of the full detector itself. If the radius were larger than the detector, the distribution would be inverted, without a single maximum. The radius of the detector is 77mm. Simulations of the voltage reading on the detector expected for cones of different radius were run, with results given in figure 9. The radius of the real cone can be approximated by comparing figure 7 with the simulation results.

These simulations assume a Gaussian distributed cone hitting the detector perpendicularly. The 10mm cone gives a signal with a central minimum in Channels 2, 3, and 4, not seen in figure 7. The 90mm cone shows the signal expected if the radius of the cone were larger than that of the detector: Channels 3 and 4 exceed Channels 1 and 2 at the centre, and a single clear maximum is no longer seen. The best estimate of the radius of the cone from the simulations is 30mm, at a distance of 0.57m from the end of the lens.

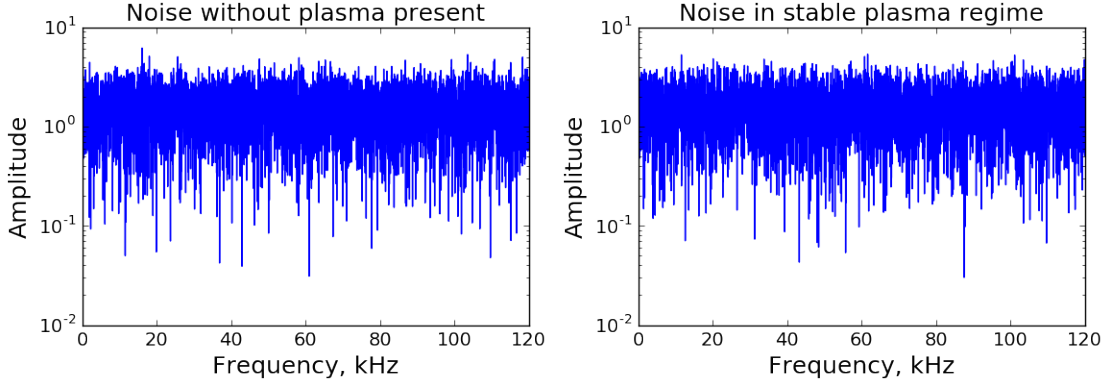


Figure 10: Fourier transform of the voltage signal for no plasma, left, and plasma in the voltage limited regime, right. The magnitude of noise is the same in both plots.

## 5.2 Stability of the Plasma

A Fourier transform of the voltage signal shows the stability of the signal over time. Peaks and increased noise in Fourier space denote greater instability, with an unstable plasma producing a greater density of high amplitude peaks. To test the stability of the plasma, the signal from the voltage sensor was converted to Fourier space with the range 0 to 120kHz visible. It is possible that other instabilities not seen here exist in the plasma, localised to higher frequencies. Figure 10 shows the Fourier Spectrum of the voltage signal, firstly, without plasma, and secondly, with plasma in the voltage limited regime below the critical magnetic field strength.

In both instances, the high voltage supply was on and set to 20kV. The noise is very low in both cases, and the two are indistinguishable. The small amount visible is due to the high voltage power supply and noise of the surrounding electronics in the lab. It is therefore clear that forming a plasma has not itself produced an instability in the tank. In contrast, the Fourier Spectrum of the voltage signal for a plasma in the current limited regime above the critical magnetic field strength is given in figure 11. Here, a large increase in noise can clearly be seen at frequencies up to 10kHz. Therefore there is a clear distinction between the stability of the voltage limited and current limited plasma regimes. At higher frequencies, no additional noise is seen.

## 5.3 Voltage Results

In exploring the possibilities for the instability of the 2015 beam test plasma, data was taken varying the strength of the magnetic field at a fixed base voltage, in order to determine the range of parameters at which a stable plasma is produced. For a given base voltage, it was found that there was a magnetic field strength below which plasma was not produced, and above which a stable, voltage limited plasma was formed. Increasing the field increased the number of ions hitting the voltage sensor, up to a critical field, at which the plasma would move to an unstable

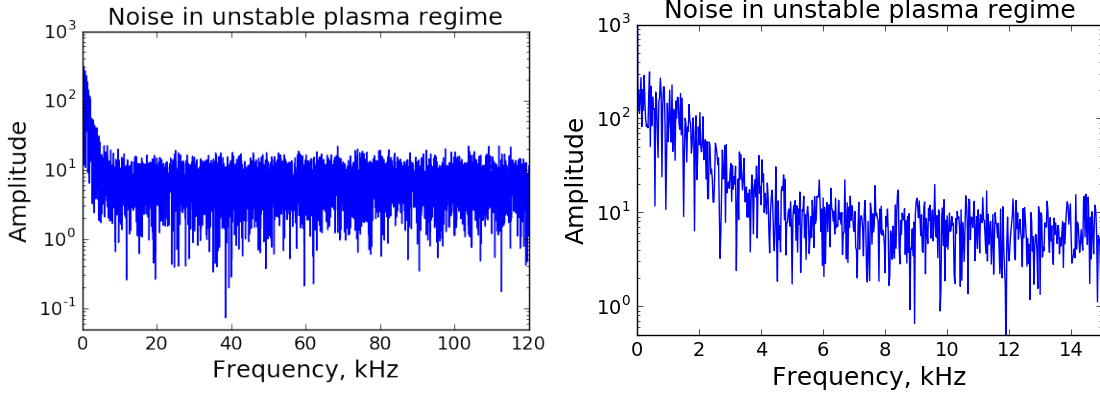


Figure 11: Fourier transform of the voltage signal for the plasma in the current limited regime above the critical magnetic field strength. The full frequency range is shown, left, and the low frequency range, right. A large increase in noise is visible in the low frequency range.

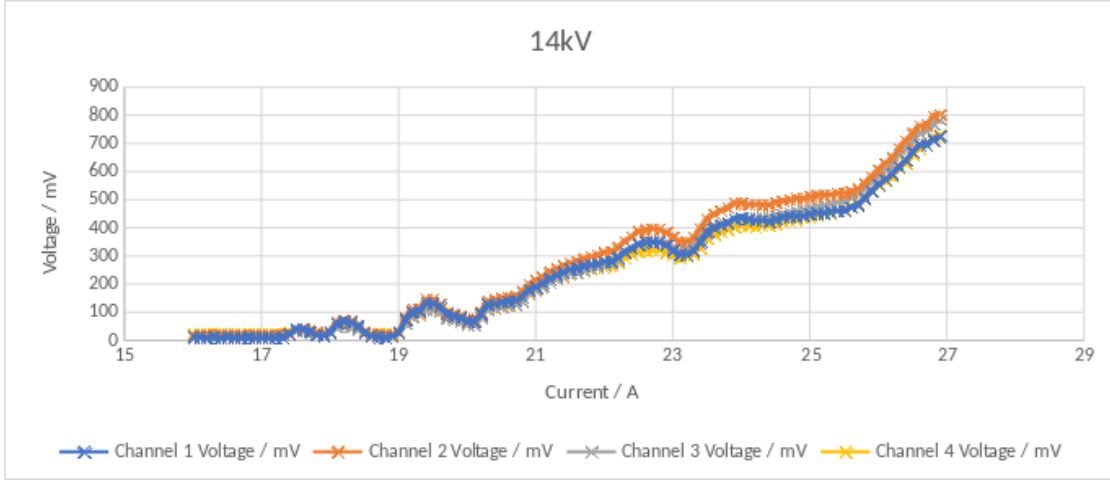


Figure 12: Sensor voltage against current through the coils for a base voltage of 14kV. The lowest input current is slightly below the limit for plasma to be produced, and the plot ends at the critical magnetic field. Above this, the plasma became unstable, and no further voltage readings could be taken. The results from all four channels of the voltage sensor are shown.

current limited regime. The instabilities were too large for a consistent voltage sensor reading to be taken above this point, and discharges from the plasma would cause the pressure to rise by multiple orders of magnitude within a few seconds. For 14kV the plot of voltage signal against current through the coils is given in figure 12. The stable plasma is first formed at 19A, although some unstable plasma is produced between 17.5A and 18.5A. The plot ends as the magnetic field becomes too large, and the unstable region is entered. In between, the number of ions hitting the sensor is seen to increase relatively linearly. The gradient of the increase changes in two regions. One possible explanation is that, in these regions, the contribution from the longitudinal expulsion of electrons lowers the measured voltage. The current of the ions on the sensor continues to increase, however the discharged electrons offset the ion contribution so that the measured current remains approximately constant.



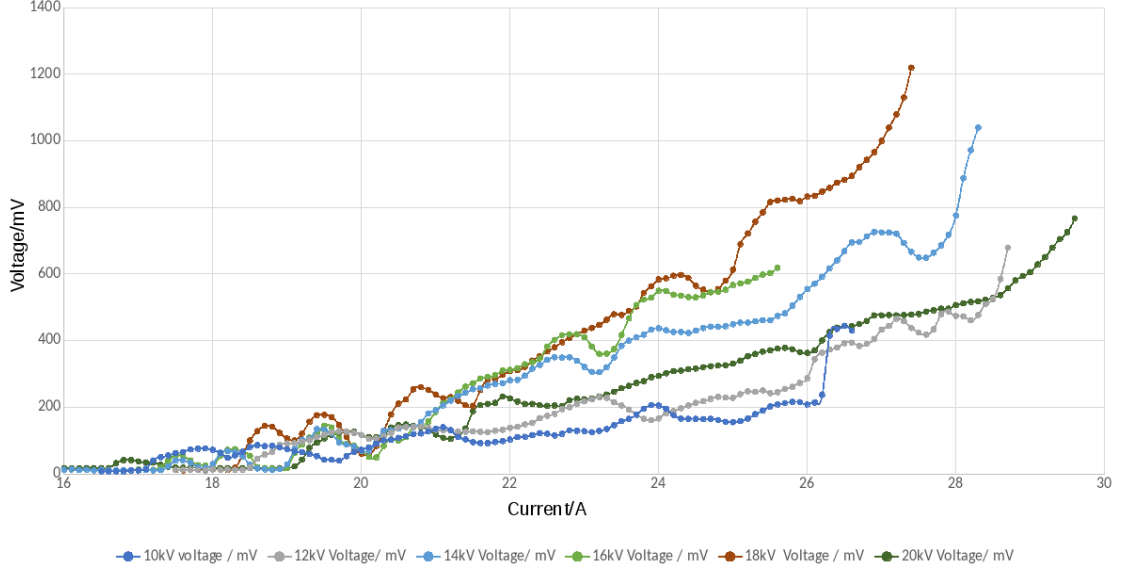


Figure 13: Sensor voltage against current through the coils for a range of base voltages 10 to 20kV.

The measurements taken at 14kV were repeated at every 2kV from 10kV to 20kV. The results are given in figure 13, for a comparison of each base voltage. The data shows that a stable plasma can be produced throughout the range of currents through the coils from 19A to 25A for all base voltages. The shape of each graph is similar, but strongly affected by small differences in pressure and temperature. If the electron filling of the lens were homogeneous, it would be expected from equations 3 and 4 that the sensor voltage would be proportional to the base voltage and the square of the magnetic field. The results here imply, therefore, that the electrons are not distributed entirely homogeneously within the lens.

## 6 Gabor Lens Beam Simulation Results

The Gabor Lens was simulated using COMSOL Multiphysics, a physics solver and simulation package. This allowed for combined simulation of the electrostatics and magnetic field in the lens. The simulation of particle beams through the lens was performed using General Particle Tracer (GPT), a beam line simulation package, and a specific Gabor Lens dedicated software created by Dr Jürgen Pozimski and described in [15].

### 6.1 Simulation of a Proton Beam

The Gabor Lens was simulated in COMSOL for an electrode potential of 20kV and an external current density of  $2.53 \times 10^6 \text{ A m}^{-2}$ . In GPT, a beam of protons of mean energy 4MeV was

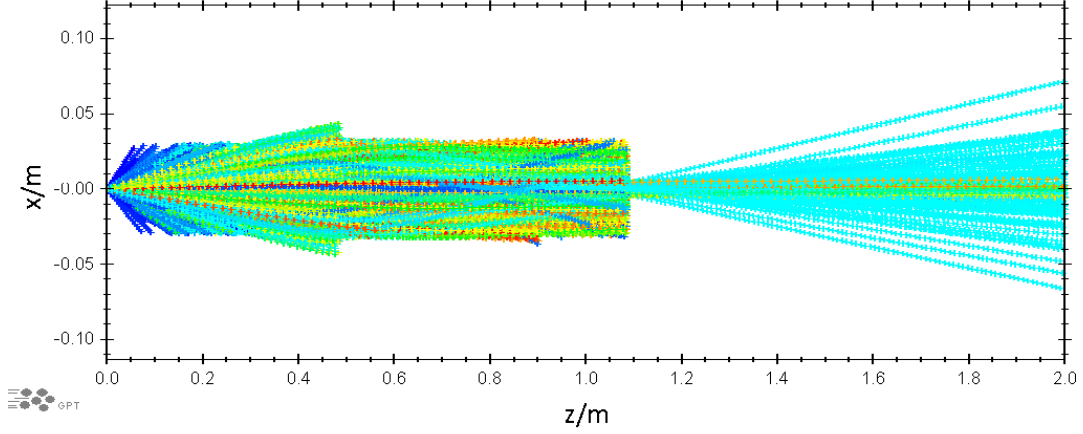


Figure 14: Results of the simulation of a proton beam travelling through the Gabor lens, a beam pipe, and aperture. The Gabor lens ranges from 0 to 0.59m in the  $z$  direction and the aperture is placed at 1.09m. The protons range in energy from 0.1MeV, in blue, to 7.4MeV in red.

simulated going through the COMSOL Gabor lens. The standard deviation of the spatial spread of the protons was 0.1mrad, and standard deviation of the energy spread 3.4MeV. After leaving the lens, the protons travel through a beam tunnel ending in an aperture 0.5m from the end lens. A density plot of the proton beam is given in figure 14. Protons of two energies pass through the aperture: those with energy 2.25MeV whose first focal point is at the aperture, and those with energy 0.47MeV which reach the aperture at their second focal point, having been focused once within the lens already. As the first focal point for these lower energy protons is within the lens, their energy is less than half that of the 2.25MeV protons. This is seen in the histogram of particle energies, given in figure 15.

## 6.2 Simulation of a Muon Beam

As discussed briefly in Section 3, in addition to proton and other ion beams, the Gabor lens may also be used to focus a muon beam. As an initial study, a muon beam was simulated for 100MeV muons, to explore whether the increase in voltage required for a focal length on the order of 1m was feasible. A monoenergetic muon beam of radius 5mm, with spatial divergence 0.001mrad was simulated. A density plot of the muon beam is given in figure 16. The focal length is found to be just 2.6m. At  $z=0$ , 5000 particles were simulated, with 450 found in the central bin. At the focal point, 3500 particles had survived, with 1100 found in the central bin. The other 1500 particles hit the edges of the beam pipe and were removed from the simulation. Further simulations were performed to calculate the base lens voltage required for a focal length of 1m as 40kV. This implies that the Imperial College Gabor Lens in its current form could be used in experiments with muon beams. The next step required will be to simulate a muon beam with more realistic spatial parameters.

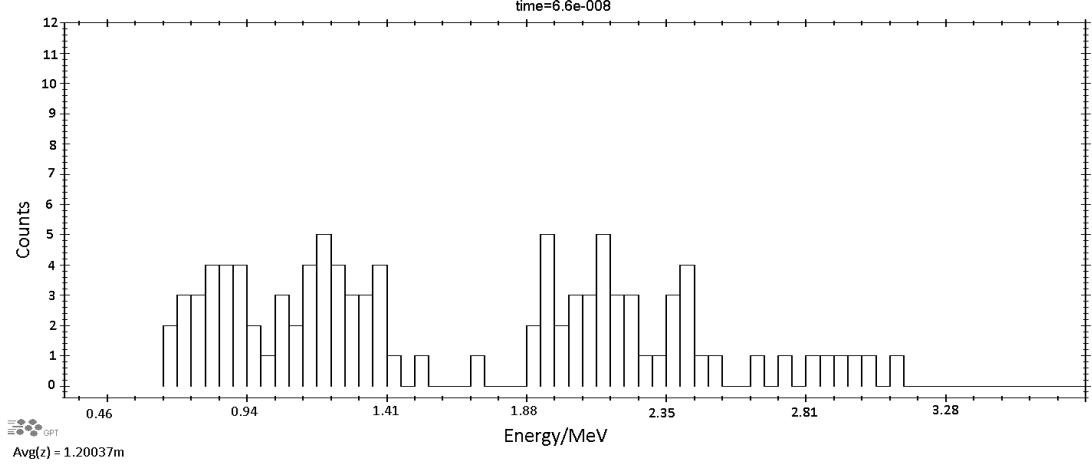


Figure 15: Energy histogram of particles at  $z = 1.2\text{m}$ , just beyond the aperture. The energies of the particles are given in terms of their Lorentz factor. Two sets of particles have survived, with average energies  $0.47\text{MeV}$  and  $2.25\text{MeV}$  respectively.

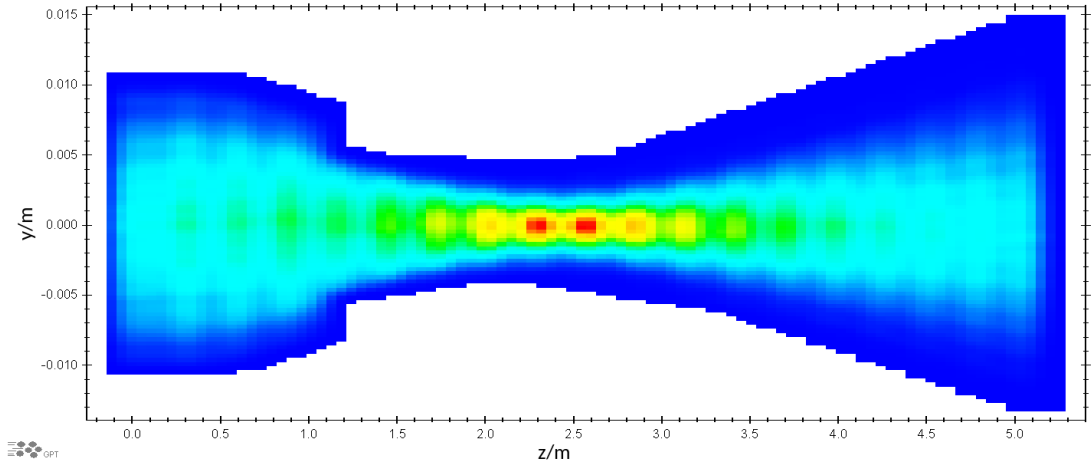


Figure 16: Density of muons travelling through the Gabor lens and beam pipe. The Gabor lens ranges from 0 to  $0.59\text{m}$  in the  $z$  direction. The highest density, in red, occurs at the focal spot, at  $2.0\text{m}$  from the end of the lens.

## 7 Conclusions and Outlook

In 2015, a beam test of the Gabor lens at the university of Surrey was performed, and pencil beams were seen to be converted into rings, due to instabilities within the plasma. Since then, work has been focussed on removing any possible sources of instability in the lens - achieving lower operating pressure and improving the configuration of magnetic coils. In the work described here, the lens was rigorously tested, and regions of stable plasma clearly identified. For given base voltages, the range of magnetic field strengths high enough for plasma to be produced, but low enough to avoid the unstable current limited regime was observed. The stability of the voltage limited regime was verified, by looking at the Fourier spectrum of the ion signal on the detector. In addition, observations made by moving the voltage sensor allowed for properties of the ion cone to be calculated. Finally, simulations were conducted of proton and muon beams being focussed by the lens. For the proton beam it was noted that protons of two independent energies were focused at on an aperture at their first and second harmonic respectively. The focal length of a 100MeV muon beam was observed as being only 2.5 times larger than that of the 4MeV proton beam for the same electric and magnetic field strengths. This demonstrates that focussing a muon beam with the Gabor lens is feasible in terms of supplying a high voltage, and should be explored in future work.

The immediate next step will be to perform a new beam test, to verify that the lens now performs in a stable manner. The experiments described here have formed the groundwork testing with a proton beam. Stable regions of plasma have been verified and the lens appears to be operating stably. Additionally, simulations of proton beams allow calculation of the focal length for protons of a given energy through a beam pipe of a given length. A proton beam test is expected in the coming months and, if successful, it will be possible to begin testing the Gabor lens focussed beam on cell samples on the road to proton beam therapy. Additionally, the possibilities for testing the Gabor lens with a muon beam are now being explored.

## References

- [1] D. Gabor. “A Space-Charge Lens for the Focusing of Ion Beams”. In: *Nature* 160 (July 1947), pp. 89–90. DOI: 10.1038/160089b0.
- [2] J Pozimski et al. “First experimental studies of a Gabor plasma-lens in Frankfurt”. In: *Proc. 3rd EPAC Conf.* 1992, p. 1536.
- [3] K Schulte et al. “Gabor Lens Performance Studies at the GSI High Current Test Injector”. In: *Proceedings IPAC* 13 ().
- [4] J Pozimski and M Aslaninejad. “Gabor lenses for capture and energy selection of laser driven ion beams in cancer treatment”. In: *Laser and Particle Beams* 31.04 (2013), pp. 723–733.
- [5] JA Palkovic et al. “Measurements on a Gabor lens for neutralizing and focusing a 30 keV proton beam”. In: *ene* 63 (1988), p. 1.
- [6] O Meusel et al. “Experimental studies of stable confined electron clouds using Gabor lenses”. In: *arXiv preprint arXiv:1309.4654* (2013).
- [7] WS Boyle and P Kisliuk. “Departure from Paschen’s law of breakdown in gases”. In: *Physical Review* 97.2 (1955), p. 255.
- [8] AA Goncharov et al. “Electrostatic plasma lens for focusing negatively charged particle beams a”. In: *Review of Scientific Instruments* 83.2 (2012), 02B723.
- [9] JR Pozimski, Morteza Aslaninejad, and Piero Antonio Posocco. “Advanced Gabor Lens Lattice for Laser Driven Hadron Therapy and Other Applications”. In: *Joint Accelerator Conferences*. 2016.
- [10] Wayne D Newhauser and Rui Zhang. “The physics of proton therapy”. In: *Physics in medicine and biology* 60.8 (2015), R155.
- [11] JA Efstathiou, PJ Gray, and AL Zietman. “Proton beam therapy and localised prostate cancer: current status and controversies”. In: *British journal of cancer* 108.6 (2013), pp. 1225–1230.
- [12] Piero Antonio Posocco et al. “First Test of The Imperial College Gabor (Plasma) Lens prototype at the Surrey Ion Beam centre”. In: *Proceedings, 7th International Particle Accelerator Conference (IPAC 2016): Busan, Korea, May 8-13, 2016*. 2016, TUPMY024. DOI: 10.18429/JACoW-IPAC2016-TUPMY024. URL: <http://inspirehep.net/record/1469967/files/tupmy024.pdf>.
- [13] U. Neuner et al. “Shaping of Intense Ion Beams into Hollow Cylindrical Form”. In: *Phys. Rev. Lett.* 85 (21 Nov. 2000), pp. 4518–4521. DOI: 10.1103/PhysRevLett.85.4518. URL: <http://link.aps.org/doi/10.1103/PhysRevLett.85.4518>.
- [14] Christopher C Davis. “Ion motion and emission profiles in low-pressure cylindrical discharges”. In: *Physical Review A* 32.6 (1985), p. 3566.
- [15] J Pozimski and O Meusel. “Space charge lenses for particle beams”. In: *Review of scientific instruments* 76.6 (2005), p. 063308.